Ohmic Flux Consumption During Initial Operation of the NSTX Spherical Torus

J. Menard[1], B. LeBlanc[1], S.A. Sabbagh[2], M. Bell[1], R. Bell[1], E. Fredrickson[1], D. Gates[1], S. Jardin[1], S. Kaye[1], H. Kugel[1], R. Maingi[3], R. Maqueda[4], D. Mueller[1], M. Ono[1], S. Paul[1], C.H. Skinner[1], D. Stutman[5], and the NSTX Research Team.

[1]Princeton Plasma Physics Laboratory, Princeton, NJ, USA
[2]Columbia University, New York, NY, USA
[3]Oak Ridge National Laboratory, Oak Ridge, TN, USA
[4]Los Alamos National Laboratory, Los Alamos, NM, USA
[5]Johns Hopkins University, Baltimore, MD, USA

Abstract. The spherical tokamak (ST), because of its slender central column, has very limited volt-second capability relative to a standard aspect ratio tokamak of similar plasma cross-section. Recent experiments on the National Spherical Torus Experiment (NSTX) have begun to quantify and optimize the ohmic current drive efficiency in a MA-class ST device. Sustainable ramp-rates in excess of 5MA/sec during the current rise phase have been achieved on NSTX, while faster ramps generate significant MHD activity. Discharges with I_P exceeding 1MA have been achieved in NSTX with nominal parameters: aspect ratio A=1.3-1.4, elongation κ=2-2.2, triangularity δ=0.4, internal inductance l_i=0.6, and Ejima coefficient C_E=0.35. Flux consumption efficiency results, performance improvements associated with first boronization, and comparisons to neoclassical resistivity are described.

1. Introduction

Spherical tokamak (ST) plasmas [1] have received considerable attention due to encouraging experimental results [2–4] from the Small Tight Aspect Ratio Tokamak (START) [5] and promising theoretical predictions regarding stability [6–9] and confinement [10]. The long-term goal of ST research is the development of steady-state configurations with high plasma β and a high fraction of bootstrap current. The compact geometry of the ST greatly limits the inductive heating and current drive capability of the ohmic heating (OH) solenoid, so the development of non-inductive current drive is crucial to the success of the concept. Nevertheless, near-term research in the ST will rely on OH current drive to generate target plasmas suitable for strong auxiliary heating to test the stability and confinement characteristics of the ST configuration. Recent experiments on the National Spherical Torus Experiment (NSTX) [11, 12] in the United States have begun to achieve high plasma current ohmically in a MA-class ST device. Typical parameters for present NSTX plasmas are: major radius $R_0 = 85$ cm, minor radius a < 68 cm, aspect ratio A=$R_0/a > 1.26$, elongation $\kappa < 2.2$, triangularity $\delta < 0.5$, vacuum toroidal field $B_T = 0.3$ Tesla at R_0, plasma current $I_P < 1$ MA, and plasma pulse length up to 0.5 seconds. Systematic scans of plasma current ramp-rate have been conducted utilizing several diagnostics and modeling tools to characterize the ohmic current drive efficiency, maximize the achievable plasma current, and to investigate the MHD instabilities observed during NSTX operation. The results of these experiments are described in the following sections. Section 2. briefly reviews the derivation of the equations used for parameterizing flux consumption, Section 3. describes the experimental results including comparisons to theory, and a summary of the results is given in Section 4.

2. Ohmic Flux Consumption

Since the ohmic solenoid flux in the ST configuration is so limited, it is desirable to quantify the relationship between the available solenoid flux, the flux at the plasma surface, and the maximum plasma current and flat-top duration achievable with these fluxes. Two different methods have been used previously to relate the poloidal flux change at the plasma boundary (denoted as $\Delta\Phi_S$) to the toroidal plasma current I_P, and a good summary of the theoretical derivation of both methods can be found in Ref. 13.

 ©2001, IAEA, Vienna

2.1. The Axial Method

The first method discussed here is commonly called the axial method [14] and was first utilized in analysis of the PLT tokamak. In this method, the change in poloidal flux at the plasma surface is split into inductive (I) and resistive (R) parts:

$$\Delta\Phi_S(t) = \Delta\Phi_I^a(t) + \Delta\Phi_R^a(t) \quad (1)$$

where

$$\Delta\Phi_I^a(t) = \Delta\Psi(t,1) - \Delta\Psi(t,0) \quad (2)$$

and

$$\Delta\Phi_R^a(t) = \Delta\Psi(t,0). \quad (3)$$

Here $\Psi = 2\pi\psi = 2\pi RA_\phi$ is the total poloidal flux integrated from the axis of symmetry of the tokamak (R=0), $\Delta\Psi(t) \equiv \Psi(t) - \Psi(t=0)$, and 0,1 are coordinates referring to the location of the magnetic axis and last-closed flux surface, respectively. The inductive flux difference $\Delta\Phi_I^a$ scales as R_0 and I_P and can be expressed in terms of a dimensionless internal inductance h_i according to:

$$\Delta\Phi_I^a = \frac{h_i \mu_0 R_0 I_P}{2}. \quad (4)$$

The inductance parameter h_i does depend on the poloidal field profile and plasma cross-section shape, but if these effects are taken into account, scaling $\Delta\Phi_I^a$ from one device to another is straight forward.

The resistive flux change $\Delta\Phi_R^a(t)$ is simply the negative time integral of the toroidal loop voltage at the magnetic axis. In so far as the on-axis loop voltage is proportional to the local resistivity, this is a useful (albeit local) measure of resistive flux consumption. In the present study, the EFIT code [15, 16] is routinely used to reconstruct the time evolution of NSTX plasma equilibria, and in principle the on-axis poloidal flux evolution can be followed. Unfortunately, internal magnetic field profile measurements were unavailable for these studies and the experimentally small $\Delta\Phi_R^a(t)$ from unconstrained EFITs does not always vary monotonically in time in the reconstructions. Such considerations motivate the more commonly used Poynting method described in the next section.

2.2. The Poynting Method

The most commonly used method of flux consumption analysis was first applied to the Doublet III device by Ejima [17]. This method is derived from a global electromagnetic power balance using the poloidal field (PF) portion of Poynting's theorem. Ignoring the time evolution of the negligible electric field energy density, power conservation dictates:

$$P_{Poynting} = P_I + P_R, \quad (5)$$

where

$$P_{Poynting} = -\int \frac{\vec{E}_\phi \times \vec{B}_P}{\mu_0} \cdot d\vec{S}, \quad (6)$$

$$P_I = \int \frac{\partial}{\partial t}\left(\frac{B_P^2}{2\mu_0}\right) dV, \quad (7)$$

$$P_R = \int J_\phi E_\phi dV, \quad (8)$$

and the volume of integration is taken to be the volume over which $\vec{J}_{Plasma} \neq 0$, i.e. the plasma volume. Here the poloidal and toroidal magnetic fields have been expressed as $\vec{B}_P = \nabla\psi \times \nabla\phi$ and $\vec{B}_\phi = F(\psi)\nabla\phi$, and the other fields have been expressed in terms of these components. As discussed in Reference 13, if the toroidal field (TF) coil current is held fixed by the TF power supply, the supply must do work against the back-EMF induced by the increasing toroidal flux of a paramagnetic plasma and net power from the TF supply crosses the plasma boundary. For NSTX plasmas which can be strongly paramagnetic by the end of the current ramp, the inductive TF power is non-negligible but is still only a small fraction of the PF heating power. This TF inductive term has been explicitly subtracted from the full Poynting's theorem in deriving Equation 5, as one is generally interested in the poloidal flux change required to generate a given plasma current.

In non-axisymmetric systems or during periods of large-scale MHD activity when axisymmetry is violated, only the total system energy is conserved and the above separation of Poynting's theorem into orthogonal field components is no longer strictly possible. In addition, some care must be taken in interpreting Equation 5, as radiation from the plasma volume is clearly included by Poynting's theorem and must be accounted for. However, any plasma species which is radiating must first have been heated resistively. Thus, plasma stored energy increases, conductive and convective losses, and radiation are all naturally included in the resistive power dissipation term $P_R = \int J_\phi E_\phi dV$.

Using the definitions of flux and field above and assuming the plasma boundary shape is held constant, it can be shown that $P_{Poynting}$ is equivalent to $I_P V_S$ where the surface voltage $V_S \equiv -\frac{d}{dt}\Phi_S$. In general, the plasma boundary shape can evolve considerably during the ramp-up phase and $P_{Poynting}$ can

deviate from $I_P V_S$. This deviation can lead to significant errors in calculations of the instantaneous ohmic heating power, but generally has a smaller impact on calculations of the flux consumed at the end of the current ramp. However, to maintain energy conservation, all subsequent calculations use a modified surface voltage defined by $V_S \equiv P_{Poynting}/I_P$. The total poloidal flux change at the plasma surface can then be expressed as:

$$-\Delta\Phi_S(t) \equiv \int_0^t V_S dt' = \Delta\Phi_I(t) + \Delta\Phi_R(t) \tag{9}$$

where

$$\Delta\Phi_I(t) = \int_0^t \frac{dt'}{I_P} \int \frac{\partial}{\partial t}\left(\frac{B_P^2}{2\mu_0}\right) dV \tag{10}$$

and

$$\Delta\Phi_R(t) = \int_0^t \frac{dt'}{I_P} \int J_\phi E_\phi dV. \tag{11}$$

In devices such as NSTX which have a small gap between the ohmic heating solenoid and the inner-most portion of the plasma boundary, the total flux-swing capability of the OH solenoid ($\Delta\Phi_{OH}$) is nearly equal to $\Delta\Phi_S$. Therefore, the relationship between $\Delta\Phi_S$ and I_P determinines the ultimate toroidal current carrying capability of the device. Because the change in flux at the magnetic axis is small during the current ramp, the change in the surface flux itself is proportional to I_P and R_0, and all three parameters can be related through a dimensionless internal inductance parameter $C \equiv \Delta\Phi/\mu_0 R_0 I_P$ computed at the end of the current ramp. By convention, the resistive flux consumption is parameterized with the Ejima coefficient $C_E \equiv \Delta\Phi_R/\mu_0 R_0 I_P$, and the total surface flux consumption is parameterized here using the Ejima-Wesley coefficient $C_{E-W} \equiv (\Delta\Phi_I + \Delta\Phi_R)/\mu_0 R_0 I_P$ [18]. For all the analysis that follows, EFIT equilibrium solutions were used to compute the volume and time integrals in Equations 10 and 11 explicitly.

Equations 9–11 above indicate that minimizing $J_\phi E_\phi$ with low resistivity and minimizing the volume-integrated B_P^2 by operating with a hollow current profile minimizes the total flux requirement for obtaining a given plasma current. However, the minimum internal inductance of the plasma is limited by MHD stability considerations, and in practice the ramp-rate of the plasma current is balanced against the resistive relaxation of the current profile to obtain the optimal current distribution. Thus, both the Ejima coefficient and the I_P ramp-rate at which it is obtained are required to make a legitimate comparison of the resistive flux dissipation of different devices.

3. Experimental Results

As discussed in the introduction, maximizing the duration of the current sustainment phase to provide target plasmas suitable for auxiliary heating is especially challenging at low aspect ratio. Since significant ohmic flux is consumed prior to the sustainment phase, plasma initiation and current ramp-up are very important phases of any tokamak discharge, and Reference 19 provides an early comprehensive review of this topic.

3.1. Plasma Initiation

Several criteria must be met simultaneously to achieve efficient tokamak initiation. First, a source for generating free electrons during the breakdown phase greatly improves breakdown reliability, and NSTX routinely uses both a biased electron-emitting filament and 10kW of 18GHz (first harmonic) ECH power to facilitate plasma breakdown at D_2 prefill pressures of 20-50 mPa. Second, a good poloidal field null is needed in the vacuum chamber to maximize the field-line connection length to the chamber walls. Work on both JET [20] and DIII-D [19] has shown that reliable current channel formation (without ECH pre-ionization) occurs if the poloidal field in the null region satisfies:

$$\frac{E_\phi B_\phi}{B_P} > 1 kV/m. \tag{12}$$

Since both E_ϕ and B_ϕ scale as 1/R, this criterion is most easily satisfied at small major radius. Thus, even though the stray poloidal field magnitude during breakdown in NSTX is pre-programmed to be less than 20 Gauss over a significant portion of the chamber volume, nearly all NSTX discharges initiate near the central column.

This start-up behavior is evident from Figure 1 which shows the typical evolution of start-up plasmas during the pre-programmed phase using a fast-framing camera [21] in early experiments on NSTX. The OH flux-swing is initiated between t=0-2msec, and a toroidal loop voltage of 4V is present at the surface of the center-stack (CS) casing by t=3-4msec. As seen in the figure, by t=7msec, the current channel has formed and the plasma is growing in volume with decreasing aspect ratio. By t=13msec, a rapid

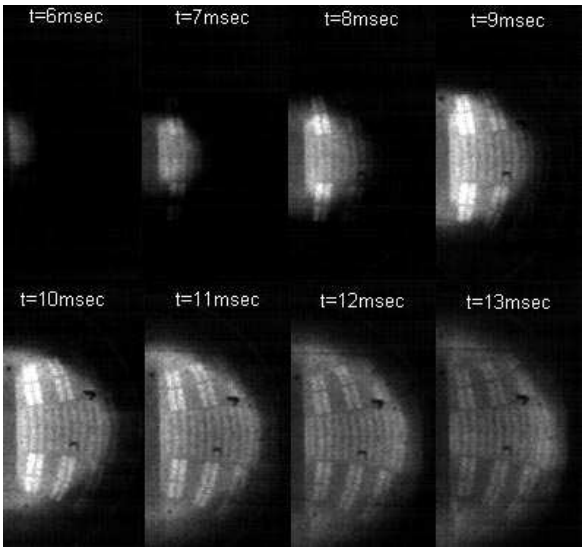

Figure 1. Visible light emission during the start-up phase of shot 100925 on NSTX using the LANL fast-framing camera.

drop in D-alpha light at the plasma boundary (not shown) indicates that the plasma has achieved full ionization. For this particular shot, the plasma has approximately the same aspect ratio and shape that it will have for the remainder of the discharge.

Lastly, the poloidal field curvature and magnitude after current channel formation must be consistent with vertical stability and radial force balance. In NSTX, the vessel toroidal eddy current can be as large as 300kA and can easily exceed the plasma current early during the ramp-up. Two independent eddy current codes [22, 23] have been used to accurately simulate this phase of the discharge to achieve efficient start-up, and both indicate that the criterion of Equation 12 has been satisfied at breakdown over a radial width spanning approximately 40cm from the surface of the central column.

3.2. Plasma current ramp-rate scans

As discussed in Section 2., flux consumption optimization is effectively equivalent to balancing the plasma current ramp-rate against the resistive relaxation of the current profile to obtain the broadest current profile that is stable to ramp-terminating MHD activity. Obviously, plasmas with different resistive dissipation require different ramp-rates to achieve the same current profile at the end of the ramp. Thus, the ability to modify the ramp-rate and control the plasma shape during the ramp is essential, especially at high plasma current. Without the recently implemented digital plasma control system (PCS) [24], achievement of the fast ramps discussed below would have been extremely difficult.

Figure 2 shows the plasma current waveforms obtained during an early I_P ramp-rate scan on NSTX. For each discharge shown in the figure, the OH, PF, and TF coil currents are pre-programmed during the first 20msec of the discharge. At t=20msec, provided that the plasma current has reached a threshold value of 100kA, coil power supply control is turned over to the plasma control system for subsequent I_P, radial position, and vertical position feedback control. The requested I_P after t=20msec was systematically increased to achieve increasingly faster ramps, and the PF shaping coil current ratios were adjusted to compensate for the higher natural elongation caused by the lower internal inductance of the faster ramps.

The systematic scans discussed above showed that sustainable average ramp-rates in excess of 5MA/sec during the current rise phase are possible in NSTX, while significantly faster ramps experience significant MHD activity. As seen in Figure 2, signatures of several different types of MHD events are apparent in the I_P traces. All ramp-rates scanned exhibited at least one late upward spike in the plasma current. This Internal Reconnection Event (IRE) [5, 25, 26] is a nearly ubiquitous feature of ST plasmas and was often associated with low loop voltage near the end of the discharge. For the fastest ramp-rates in the scan (6, 8, and 10 requested MA/sec), early large MHD events terminated the ramp and the plasma current seldom exceeded its pre-event value. Slower ramp-rate discharges generally terminated either due to insufficient loop voltage and/or OH flux. The optimal ramp-rate of 5MA/sec was just slow enough to avoid early MHD activity that terminated the current ramp.

EFIT analysis of theses disharges has been used to track the plasma shape, normalized internal inductance l_i, and Ejima coefficients during the ramp-up. The normalized internal inductance used here is defined as:

$$l_i \equiv \frac{\langle B_P^2 \rangle_V}{\langle B_P \rangle_l^2} \tag{13}$$

where

$$\langle B_P^2 \rangle_V \equiv \frac{\int B_P^2 dV}{\int dV}, \tag{14}$$

$$\langle B_P \rangle_l \equiv \frac{\int \vec{B} \cdot d\vec{l}}{\int dl}, \tag{15}$$

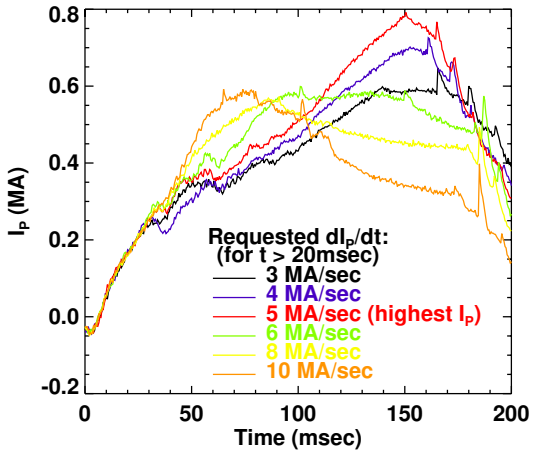

Figure 2. Plasma current traces obtained during a systematic scan of the plasma current ramp-rate.

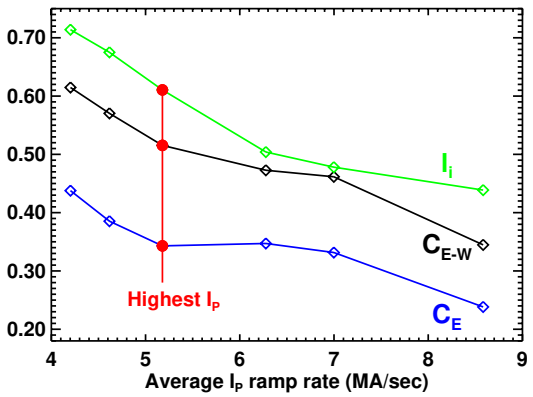

Figure 3. Internal inductance and Ejima coefficients at peak plasma current as a function of I_P ramp-rate for the discharges of Figure 2.

and $\int dV$ and $\int dl$ refer to the plasma volume and plasma boundary poloidal circumference respectively. For the shots shown in Figure 2, the PCS was used to keep the plasma shape inner-wall limited throughout most of the ramp with $A \approx 1.3, \kappa \approx 2 - 2.2$, and $\delta \approx 0.4$. The two highest current discharges in the figure became double-null diverted from t=110 to 150msec. The internal inductance typically increased during these discharges from l_i=0.2-0.3 initially to 0.6-1.0 at the time of maximum current.

Figure 3 shows that the internal inductance at peak current drops by roughly 40% as the average ramp-rate doubles from 4 to 8MA/sec. In addition, this figure shows that lower normalized resistive and total flux consumption was achieved with faster ramps. A noteworthy feature of Figure 3 is that even though the internal inductance drops significantly, most of the drop in total flux consumption with increasing ramp-rate comes from a drop in the resistive component. This is because the inductive portion of the total flux is only 30% of the total at the end of the current ramp. This implies that either the resistive consumption is considerably higher at low aspect ratio, that the inductive consumption is always smaller due to the smaller major radius and lower absolute inductance of the ST, or both.

The most relevant C_E value is that obtained at the highest I_P, and for early NSTX experiments in deuterium, shots optimized for minimal flux consumption had C_E = 0.4-0.45 and C_{E-W} = 0.5-0.6. For comparison, for low loop voltage ramp-up to I_P=1MA in the DIII-D tokamak [19], dI_P/dt = 1-1.5MA/sec, C_E= 0.5 and C_{E-W}=0.9. Values similar to these have been predicted for ITER [27] using the Tokamak Simulation Code (TSC) [28]. Thus, while low aspect ratio tokamaks do have considerably less solenoid flux available, the lower C_{E-W} parameter found in NSTX does imply that some of this loss is recovered in the ST configuration because the inductive flux required to reach a given plasma current is reduced.

3.3. Initial high current discharges

The highest plasma current achieved during the initial phase of NSTX operation was 1MA. Implementation of the full OH capability of NSTX and partial vacuum vessel bake-out were crucial in reaching this physics goal. Plasma parameters at peak I_P from EFIT reconstructions were: A=1.28, κ=1.9, δ=0.4, l_i=0.7, C_E=0.4, and C_{E-W}=0.55. One of the more interesting aspects of the 1MA shots is the reproducible plasma current "hesitation" observable on the experimental I_P traces shown in Figure 4 near t=60msec. Operationally it was found that 1MA could only be achieved by forcing this MHD event to occur early by ramping faster than 5MA/sec. This allowed the plasma to recover in such a way that no subsequent MHD was excited until the late reconnection events which occur after t=170msec. Plasma current ramp-rates both faster and slower than 7MA/sec again led to ramp-terminating MHD activity (see Figure 6). The hesitation event in Figure 4 consumed a significant fraction (20%) of the OH flux and clearly reduced the achievable I_P flattop duration. An important finding evident from Figure 3 and from analysis of the shots in Figure 4 is

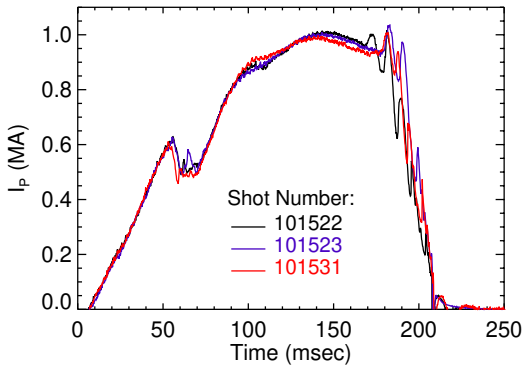

Figure 4. Plasma current traces for 1MA discharges from initial experiments in NSTX.

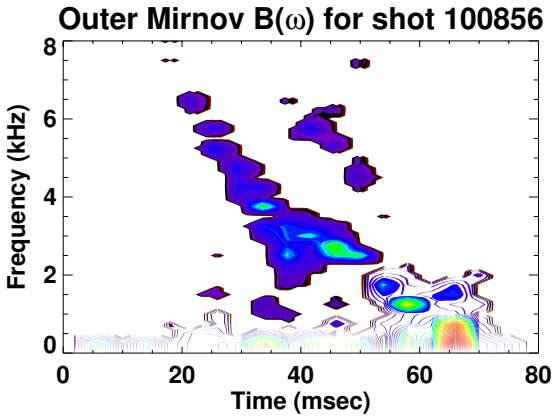

Figure 5. Outboard Mirnov frequency spectrum during the ramp-up phase of shot 100856.

that Ejima coefficients in the expected range of 0.4 were only obtained with relatively fast I_P ramps even after (partial) vessel bake-out. Several possible dissipation mechanisms responsible for this are discussed below.

3.3.1. Tearing activity

Many NSTX discharges exhibited coherent m=2 Mirnov fluctuations with decreasing mode frequency early in the plasma current rise-phase. This behavior may be indicative of the formation of locked (possibly double) tearing modes, and such modes may have dissipated OH flux during the ramp-up in many NSTX discharges. Figure 5 shows the frequency spectrum of a Mirnov sensor on the outboard mid-plane during the early phase of the 8MA/sec discharge of Figure 2 (shot 100856). The mode frequency clearly decreases from 6kHz shortly after breakdown and approaches zero within 40msec, apparently locks, and then grows rapidly near t=65msec. Not every discharge exhibits such strong locking behavior, although many show at least indications of such activity. Better density control, a slower current ramp-rate, and slower plasma expansion during the pre-programmed phase have all been tried with some success to eliminate these modes. Locked mode detector coils are presently being installed to better characterize the modes.

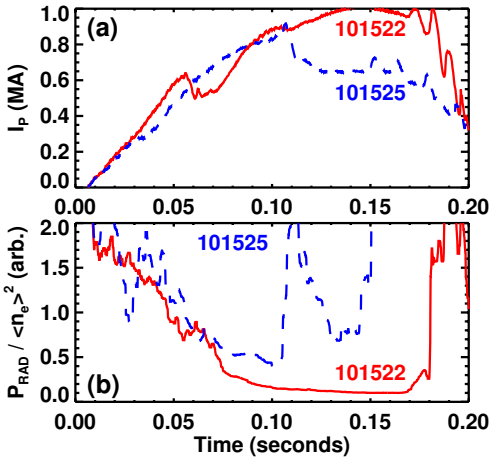

Figure 6. (a) Plasma currents for a 1 MA shot and a failed 1 MA attempt (b) Density-normalized radiated power traces.

3.3.2. Resistivity

The most obvious dissipation mechanism is plasma resistivity, and aside from the predicted neoclassical enhancement of the parallel resistivity due to increased particle trapping, soft X-ray and bolometer signals often showed an emission profile highly peaked on axis in the energy band dominated by metallic impurities. Figure 6 compares plasma current and density-normalized radiated power traces for a successful 1 MA discharge and a 1 MA attempt which failed due to a delayed early MHD event. The only difference between these two shots is the early time history of the requested I_P which modified the applied loop voltage after t=30 msec. The 850 kA peak plasma current trace (shot 101525) in Figure 6a indicates a reconnection event at t=103 msec, and Figure 6b shows that a potentially important difference between these shots is the significant decrease in the density-normalized radiated power of shot 101522 after its first MHD event. This is in contrast to the rapid rise in radiated power after the first event of shot 101525. EFITs (using only